Synchronized slice viewing of similar image series

Sharib Ali[ac], Antonio Foncubierta[a], Adrien Depeursinge[ab], Fabrice Meriaudeau[c], Osman Ratib[d], Henning Müller[ab]

[a]University of Applied Sciences Western Switzerland (HES–SO), Sierre, Switzerland;
[b]Medical Informatics, University Hospitals & University of Geneva, Switzerland;
[c]University of Burgundy, Le Creusot, France;
[d]Nuclear Medicine, University Hospitals of Geneva, Switzerland

ABSTRACT

Comparing several series of images is not always easy as the corresponding slices often need to be selected manually. In times where series contain an ever–increasing number of slices this can mean manual work when moving several series to the corresponding slice. Particularly two situations were identified in this context: (1) patients with a large number of image series over time (such as patients with cancers that are monitored) frequently need to compare the series, for example to compare tumor growth over time. Manually adapting two series is possible but with four or more series this can mean loosing time. Having automatically the closest slice by comparing visual similarity also in older series with differing slice thickness and inter slice distance can save time and synchronize the viewing instantly. (2) analyzing visually similar image series of several patients can profit from being viewed in a synchronized way to compare the cases, so when sliding through the slices in one volume, the corresponding slices in the other volumes are shown. This application could be employed after content–based 3D image retrieval has found similar series, for example. Synchronized viewing can help finding or confirming the most relevant cases quickly.

To allow for synchronized viewing of several image volumes, the test image series are first registered applying affine transformation for the global registration of images followed by diffeomorphic image registration. Then corresponding slices in the two volumes are estimated based on a visual similarity. Once the registration is finished, the user can subsequently move inside the slices of one volume (reference volume) and can view the corresponding slices in the other volumes. These corresponding slices are obtained after a correspondence match in the registration procedure. These volumes are synchronized in that the slice closest to the original reference volume is shown even when the slice thicknesses or inter slice distances differ, and this is automatically done by comparing the visual image content of the slices. The tool has the potential to help in a variety of situations and it is currently being made available as a plugin for the popular Osirix image viewer.

Keywords: global registration, deformable registration, mutual information, information retrieval, synchronized viewing

Further author information: (Send correspondence to Henning Müller, Email: henning.mueller@hevs.ch)

Medical Imaging 2012: Advanced PACS-based Imaging Informatics and Therapeutic Applications, edited by William Boonn, Brent J. Liu, Proc. of SPIE Vol. 8319, 83190K · © 2012 SPIE
CCC code: 1605-7422/12/$18 · doi: 10.1117/12.911233

1. INTRODUCTION

Medical imaging has evolved strongly over the past 20 years. The number of images has increased as has the variety of imaging protocols and differing image producing devices, contrast agents and image processing tools.[1] Most of the growth has been in tomographic images that acquire an ever–increasing number of slices. Viewing such slices is basically impossible with scanners producing hundreds or thousands of images per patient. Tools such as the Osirix platform have been created for convenient image viewing.[2]

Evaluation of large image series by the clinicians is a difficult task as much information needs to be integrated. Comparative analysis of a given series with past series of the same patient or with similar cases of different patients can be time consuming if done manually as the image slices have to be synchronized. Irrespective of scanning techniques (modality), orientations or slice thickness, it would be good to find locations in similar image series belonging to same area that are automatically located to ease the follow up of infections, tumor growth or any other abnormality. Such a tool can be a good complement to 3D retrieval of similar cases,[3,4] which is basically an extension of content–based image retrieval, having received much research attention over the past 20 years.[5–7]

The work described in this article applies a robust image registration technique for this objective in a first step. Image registration is a process to change the appearance of the images relative to a reference image by finding a transformation that can rotate, translate and stretch images, thus enabling direct comparisons, combination or analysis.[8] The registration can find a transformation between two images. Based on the nature of the transformations, the registration can be categorized as *rigid*, *affine* or *elastic*. The transform obtained from rigid registration is characterized by rotation and/or translation parameters. Affine registration includes shear parameters in addition to rotation and translation. In this article, both rigid and affine registration methods are used to globally register the images. The techniques consist of an approximate transform for correcting the global differences in position, orientation and shear between the reference volume and the test volumes. In a second step, the registration is refined using elastic registration (also called deformable registration) that is able to express both global and local deformations.

This paper describes the implemented registration pipeline and shows the results of the registration of lung computed tomography (CT) and brain magnetic resonance imaging (MRI) in particular. The implemented methodology is intended to focus on possibilities and results regarding the image registration that is useful for efficient correspondence matching problems. Most of the brain images could be registered easily using a rigid or affine transformation. However, it is not as easy to get a good correspondence with the lung images using such transformations. A non–linear registration technique is required for these soft tissue deformations and was implemented mainly for lung CT image alignment. The idea was to get a non–linear transform, which could be used to model the local deformation after applying a global linear transform. The implemented non–rigid deformable transformation works well with major anatomical structures. Similarity metrics are the key for evaluating the correspondences and these have to be identified.[9,10] Mutual information was used as a similarity metric.[11] In order to accelerate the computation the images are first downsampled. A rigid transformation was applied to this downsampled image series and the registration of the image series was initiated. The transformation obtained is then used to initialize the affine transformation with more degrees of freedom. These steps consist of the global positioning of the images. The bulk transform obtained from the global registration is used to initialize a B–spline deformable transformation with a higher degree of freedom. B–spline deformable transformations are split into coarse and fine registration proce-

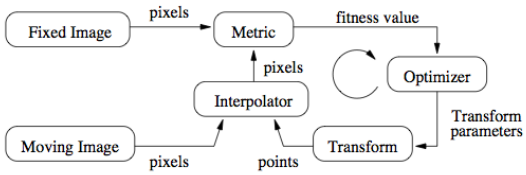

Figure 1: *Block diagram with the components of the registration.*

dures making use of a multi–resolution image registration concept. The optimizer maximizes the mutual information between the two image series.

We also developed a plugin of our system for Osirix* using the ITK† (Insight Toolkit) registration libraries for an efficient image registration of major parts of body. This availability within Osirix should make the tool available for a larger number of physicians. The objective is to make the system fully automatic and robust for aligning image series of various body parts with respect to a single image series. This should not require any manual segmentation or annotation of the structures. Automatic navigation in similar image series is the prime objective. Finding the correct slice automatically in other registered series with respect to one reference series is required for such a navigation.

2. METHODS

Image registration is the process of determining the spatial transformation that maps similar points from one image to another image. Registration is basically treated as an optimization problem with the goal of finding the best transformation that aligns a new image also named a template image, source image or test image with respect to a fixed image also referred to as reference image or target image. In this article, the term test image is employed, and fixed image for the reference image series. The basic framework with components of image registration is shown in Figure 1. The fixed image $f(\boldsymbol{x})$ and the test image $m(\boldsymbol{x})$ are the input images with $\boldsymbol{x}$ representing the n–dimensional coordinates. The transformation component $T(\boldsymbol{x})$ gives the spatial mapping points from one image to the other while the interpolator $I(\boldsymbol{x})$ evaluates the test image intensities at non–grid positions. The interpolator function is the first fundamental part of the registration that defines the images in continuous spatial coordinates. The associated transformation function $T{:}\Omega_f \rightarrow \Omega_m$, where, $\Omega_f \subset R^3$ and $\Omega_m \subset R^3$ with Ω_f and Ω_m represents fixed and moving regions respectively. An anatomical structure present in the fixed image in a point $\boldsymbol{x} \in \Omega_f$ is mapped to the corresponding point in the test image at $\boldsymbol{y} \in \Omega_m$ using the transformation function $T(\boldsymbol{x}) = \boldsymbol{y}$. From the obtained transformation function, deformation vectors of every voxel in the fixed image can be calculated as $d(\boldsymbol{x}) = \boldsymbol{y} - \boldsymbol{x}$. A metric is used to evaluate the (dis)similarity between the test and the fixed image. An optimizer is required in image registration to search for the optimum transformation that maximizes the similarity between the images. Thus, the optimization method needs to minimize a given cost function (i.e., finding the best possible transformation that defines point–to–point correspondence between the two images). Mutual information was used as a metric to quantify the matching between the two images. It is also used by the optimizer for finding the best transformation. Mutual information measures the information that two volumes share. Registration is executed by maximizing that information and involves finding a transformation from the coordinate frame of one to the other

*http://www.osirix-viewer.com/
†http://www.itk.org/

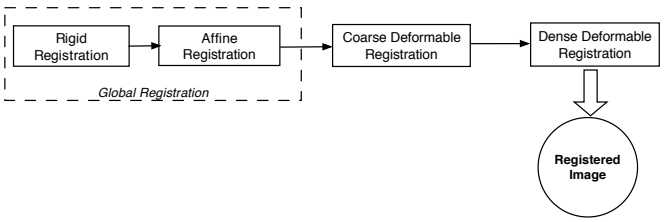

Figure 2: *Pipeline of the implemented registration*

image volume such that it maximizes the mutual information I between the two. It can be stated as a maximization problem.

$$\underset{T}{\operatorname{argmax}}(I(f(\boldsymbol{x}), m(T(\boldsymbol{x}))). \tag{1}$$

Mutual information is defined in terms of entropy as:

$$I(f(\boldsymbol{x}), m(T(\boldsymbol{x}))) = h(f(\boldsymbol{x})) + h(m(T(\boldsymbol{x}))) - h(f(\boldsymbol{x}), m(T(\boldsymbol{x}))), \tag{2}$$

where h is the entropy of a random variable and is defined as $h(x) = -\int p(x)\ln(p(x))\mathrm{d}x$, p is the probability and $h(x, y)$ the joint entropy of two random variables x and y as:

$$h(x, y) = -\int p(x, y)\ln\ (p(x, y))\,\mathrm{d}x\,\mathrm{d}y. \tag{3}$$

First term on the right of Eq. (2) is the entropy in the fixed volume, second term is the entropy of the part of the moving volume into which the reference volume projects. The third term, the (*negative*) joint entropy of f and m, contributes when both are functionally related. The last two terms identify transformations that explain the information in both volumes.

The implemented registration pipeline consists of four major steps (see Figure 2) and uses the mutual information as similarity metric. The first two steps globally align the image volumes using rigid and affine registration methods. Then, a coarse deformable registration is done and in the final step dense deformable registration is implemented for refining the results. Two separate deformable registration steps are applied to deal with large image series. The first three steps are performed at lower resolution and then in the final step the transformation is used as the start for registration at higher resolution.

2.1. Rigid Registration

A rigid registration $\boldsymbol{T}_R(\boldsymbol{x})$ finds the optimal parameters (i.e., three rotations and three translations) that globally maximize the mutual information between the two images using multi–resolution stochastic gradient descent optimization. This exploits the over constrained problem of rigid registration as the number of voxels is much larger than the transformation parameters.[12] A small random sample of the image domain is used at each iteration. For each iteration, the number of voxel samples chosen was 10^4 and 50 grey–level histogram bins were used to find the mutual information for the optimizer. A regular step gradient descent optimizer was used. At each iteration this optimizer takes a step size of 0.01 in the negative direction of the gradient. A local extremum is assumed when the gradient changes direction abruptly and the step length is decreased by the optimizer. It is important to set the number of iterations for convergence because the optimizer may fluctuate between the maxima and minima of the function. We have set it to 50 iterations.

2.2. Affine Registration

Affine registration $\boldsymbol{T}_A(\boldsymbol{x})$ is used to get the transformation that is optimized with respect to translation, rotation, scaling and shearing. It is initialized by using the transformation obtained from the rigid registration step. In this case, another 20 iterations are executed taking 5×10^4 voxel samples with 50 histogram bins.

2.3. Deformable Registration

The global registration (rigid and affine registration) accounts only for differences due to position, orientation and size of the anatomy but it cannot deal with small anatomical changes between subjects. To overcome this problem it is necessary to employ a non–rigid transformation.[13] A series of N B–spline transformations[14] are applied to the pre–aligned images. The final transformation is therefore a composition of transformations obtained from the global registration step and N levels of B–spline transformations.

$$\boldsymbol{T}_{\text{final}}(\boldsymbol{x}) = \boldsymbol{T}^{N}_{\text{B-spline}}(\boldsymbol{x}) \circ \ldots \circ \boldsymbol{T}^{1}_{\text{B-spline}}(\boldsymbol{x}) \circ \boldsymbol{T}_A(\boldsymbol{x}) \circ \boldsymbol{T}_R(\boldsymbol{x}), \tag{4}$$

where $\boldsymbol{x}$ is a point in the fixed image domain Ω_f and "$\circ$"denotes the transformation composition. The 1D basis function of a B–spline is a piecewise polynomial with a uniform spacing between the control points. This is extended to higher dimensions by a tensor product. A B–spline deformation field in 3D is defined as:[14]

$$\boldsymbol{T}_{\text{B-spline}}(x,y,z) = \sum_{l=0}^{3}\sum_{m=0}^{3}\sum_{n=0}^{3} B_l(u)B_m(v)B_n(w)\boldsymbol{c}_{i+l,j+m,k+n}, \tag{5}$$

where, (x, y, z) are the spatial 3D image coordinates, $\boldsymbol{c}$ is a uniform grid $n_x \times n_y \times n_z$ of control points used to parameterize the transformation with $i = \lfloor x/n_x \rfloor - 1$, $j = \lfloor y/n_y \rfloor - 1$, $k = \lfloor z/n_z \rfloor - 1$, $u = x/n_x - \lfloor x/n_x \rfloor$, $v = y/n_y - \lfloor y/n_y \rfloor$, $w = z/n_z - \lfloor z/n_z \rfloor$, and B_q are the q^{th} B–spline basis functions as:

$$B_0(u) = (1-u)^3/6, \tag{6}$$
$$B_1(u) = (3u^3 - 6u^2 + 4)/6, \tag{7}$$
$$B_2(u) = (-3u^3 + 3u^2 + 3u + 1)/6, \tag{8}$$
$$B_3(u) = u^3/6. \tag{9}$$

The optimal transformation is obtained by minimizing the cost function associated with both the global and local transformation parameters. This cost function contains: 1) the cost associated with the voxel–based similarity measure (i.e., mutual information) and 2) a regularization term, which constraints the transformation to be smooth.[14] The cost function C that the registration algorithm minimizes is defined as

$$C = -\bar{I} + \lambda||\nabla \boldsymbol{U}||, \tag{10}$$

where $\bar{I}$ is the normalized mutual information, $||\nabla \boldsymbol{U}||$ denotes the L_2–norm of the gradients of a smooth deformation field $\boldsymbol{U}$, and λ is a weighing factor that controls the relative strength of the term. The optimal deformation field $\boldsymbol{U}$ is computed iteratively as:

$$\boldsymbol{U}^n = \boldsymbol{U}^{n-1}(\boldsymbol{Id} + \boldsymbol{T}^n_{\text{B-spline}}) + \boldsymbol{T}^n_{\text{B-spline}}, \tag{11}$$

where $\boldsymbol{Id}$ denotes the identity matrix and $\boldsymbol{T}^n_{\text{B-spline}}$ is a local update at the n^{th} iteration, which is computed at each iteration to maximize the mutual information between the fixed and the deformed test image volume.

The computational cost while dealing with such non–linearities can be decreased by using a multi–resolution approach as in.[15] This multi–resolution technique used for applying a non–rigid B–spline registration has three levels of B–spline transformations ($N = 3$) with decreasing grid size used. First, coarse deformable registration was executed by taking grid cells of $5 \times 5 \times 5$ adopted in a multi–resolution approach. Finally, this deformed transformation was used for fine deformable registration. The grid size was taken to be as large as $20 \times 20 \times 20$ and applied to the full resolution image. To make the registration process faster, only 7 iterations were done in this final step.

2.4. Data set used

An existing data set with 15 image series pairs was taken from several sources to evaluate the proposed system. The data set includes 10 pairs of chest computed tomography (CT) series. The remaining 5 series were from Magnetic Resonance Imaging (MRI) of the brain. Among the 10 pairs of lung CT images, 7 pairs are from the database of the EMPIRE10 registration challenge[‡]. The series in this data set have identical interslice distance between the fixed and test image series. The remaining 3 pairs were taken from a database of cases used with Osirix[§] with different inter–slice distance and slice thickness. These images were not categorized into fixed and test image pairs in contrast to the data set from the previous database. In order to evaluate the system accuracy for other modalities and anatomic regions, MRI brain images were used as well. The MRI data set was also taken from cases made available with Osirix. Thus, 15 pairs of image series were used for the evaluation of the system accuracy.

EMPIRE10 has images taken from a single subject but taken with a variety of sources including varying institutes with varying scanners and protocols. We chose 5 pairs of lung CT images having 0.7mm isotropic resolution and one each with 0.6mm and 1.5mm. Scans included in the data set are taken at various phases of the breathing cycle.[16]

Lung images from the Osirix database were chosen such that the interslice distance and slice thickness in the series to be registered was large. Image series with a slice thickness 3mm, 3mm, 1mm and 3mm with interslice distances 3mm, 1.5mm, 0.5mm and 0.5mm respectively were chosen. These image series were registered keeping one image series as fixed and the other (chosen randomly) as the test series to evaluate registration for image series with varying slice thickness and interslice distances.

A brain dataset with the name BRAINIX was used. Among the 7 series in this dataset, 5 image series with limited noise were used for the evaluation. The dataset included both T1, $T2^*$ and T2 weighted MR images. Four image series had a slice thickness of 5mm and the remaining one had 1mm.

3. RESULTS

First, a gold standard was created by manually setting the reference points in the image series. The reference points chosen were the apex of the lung, tracheal splitting and uppermost slice showing the diaphragm in the lung CT. For brain MRI images, reference points are the top of the head, top of the cerebellum and the bottom of the cerebellum. These series were then registered keeping one of the image series as fixed and the other as the test series. The automatic alignment of the image volumes with the fixed volume was achieved after registration (see Figure 3). The difference between the slice corresponding to the manually set reference point and the slice obtained after automatic alignment of the registered image series is the error. The error in the

[‡]`http://empire10.isi.uu.nl/download.php` last visited 1.11.2011

[§]`http://pubimage.hcuge.ch:8080/`

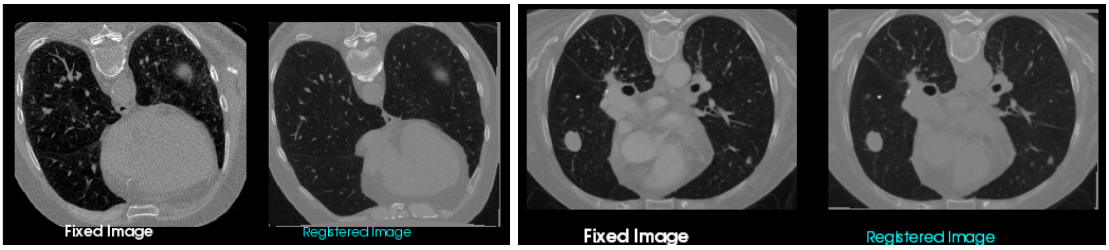

Figure 3: *Automatic alignment of two registered lung CT pairs.*

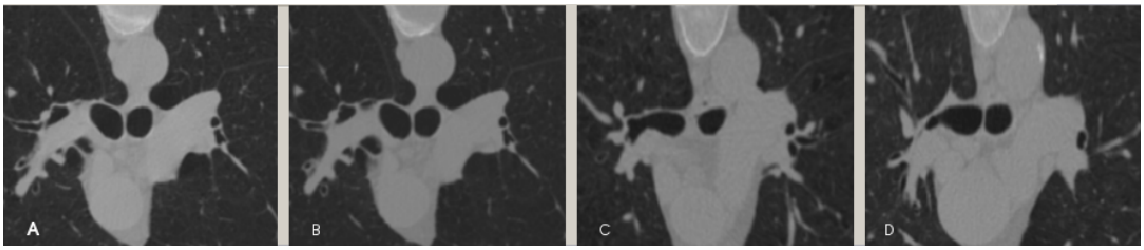

Figure 4: *Three image series (B, C, and D) registered with image series A. Tracheal splitting in the fixed image A with similar automatic synchronization in other image series after registration shown in views B, C and D. In C there is an error of 2.1mm (3 slices) while the others have no error. CTs of different patients were taken into account. The interslice distance of each series is 0.7mm with a slice thickness of 1mm*

registered volumes in the registered image series is taken only along the z–direction (*axial*). This means that if two image series A and B have an inter slice distance of 0.7mm and B is to be registered with respect to A, then after the registration the reference point in the ground truth corresponds to slice 12 in A but the same reference is on slice 10 of B, and the error measured is $2 * 0.7 = 1.4mm$. Similar calculations were performed for all the reference points and the mean was calculated for each pair of image series as shown in Table 1.

Our main objective is to align several image series of the same or different patients with a single fixed image series (reference series) as shown in Figure 4. Here, series A is taken as fixed series and the remaining three B, C and D are considered as test image series. An example of registered brain MRIs is shown in Figure 5 after implementing registration with only 2 iterations in the fine deformable registration. Decreasing the number of iterations in the fine deformable registration improves computational complexity.

The time taken for the registration of these three test series to get aligned with the fixed series is optimized by setting different parameters (e.g., the number of iteration steps in fine registration) in order to find a trade–off between execution time and convergence error. The time required to achieve convergence (in other words synchronize) is 2 minutes 35 seconds on a Mac OS X portable computer with a 2.3GHz Intel Core i5 processor and 4GB of RAM.

4. INTERPRETATION

Registration is clearly required to obtain automatic alignment of two or more image volumes, which can help in synchronized viewing of several similar image series together. We implemented the treatment pipeline using ITK libraries and also developed an Osirix plugin to make the tools potentially available for a larger group of users.

Table 1: *Error in mm for the evaluation of accuracy in automatic alignment. The mean error for lung image series and brain image series are 3.95mm and 0mm, respectively.*

Scan pair	Interslice distance (mm)	Slice thickness (mm)	Error (mm)	Mean error (mm)
A. Lung Pair				
1	0.7 0.7	1 1	Apex: 2.1 Trachea split: 0.7 Diaphragm: 0.7	1.16
2	0.7 0.7	1 1	Apex: 1.4 Trachea split: 0.7 Diaphragm: 0.7	0.933
3	0.7 0.7	1 1	Apex: 0 Trachea split: 0 Diaphragm: 0.7	0.233
4	0.6 0.6	1 1	Apex: 0 Trachea split: 2.4 Diaphragm: 0.7	1.03
5	0.7 0.7	1 1	Apex: 0 Trachea split: 0 Diaphragm: 0	0
6	1.5 1.5	1 1	Apex: 0 Trachea split: 0 Diaphragm: 0	0
7	0.7 0.7	1 1	Apex: 1.4 Trachea split: 0.7 Diaphragm: 0.7	0.933
8	3 0.5	3 1	Apex: – Trachea split: 6 Diaphragm: 0	3
9	0.5 3	1 3	Apex: – Trachea split: 11 Diaphragm: 0	5.5
10	3 1.5	3 3	Apex: – Trachea split: 0.7 Diaphragm: 0	3.75
B. Brain Pair				
1	5.98 5.98	5 5	Top of head: 0 Top of cerebellum: 0 Bottom of cerebellum: 0	0
2	-5 5.98	5 5	Top of head: 0 Top of cerebellum: 0 Bottom of cerebellum: 0	0
3	-5 -5.98	5 5	Top of head: 0 Top of cerebellum: 0 Bottom of cerebellum: 0	0
4	1 5.98	1 5	Top of head: 0 Top of cerebellum: 0 Bottom of cerebellum: 0	0
5	-5 1	5 1	Top of head: 0 Top of cerebellum: 0 Bottom of cerebellum: 0	0

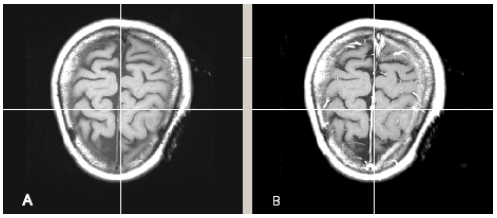

Figure 5: *Automatic alignment of brain images (top of brain).*

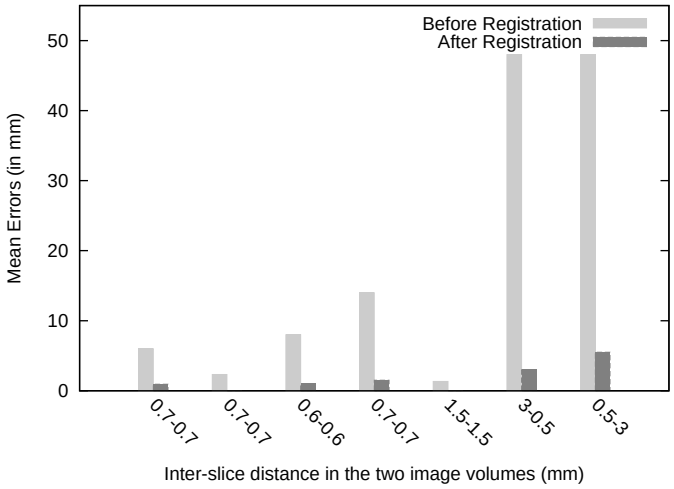

Figure 6: *Error comparison for distances in similar slice in the two volumes (before and after registration).*

Figure 6 shows the misalignment in two image volumes before and after registration. Two image volumes with the same and a differing interslice distance were used in this case. The image series were chosen such that their first slices were initially aligned to the same point. We then manually navigated into the image series along the z–direction for all the reference points (i.e., apical region, top of the diaphragm and splitting of the trachea). The mean of the misalignments before the registration was used as a baseline. Similarly, we calculated the misalignment as a distance for the registered pair. It is clear that the slices are highly misaligned before registration. The series are effectively aligned with only negligible distance between image pairs after registration in most of the cases. However, the misalignment was comparatively large for the volumes with a large difference in the inter slice distances.

Table 1 also contains the detailed errors for all the analyses. From Figure 7 it is clear that the apical region and diaphragm of lungs were registered with a very small error ($\sim$0.7mm and 0.35mm respectively) while the tracheal splitting has a higher error ($\sim$3mm). The top of the lungs (i.e., apical region) and the diaphragm (nearly at the bottom of the series) form clear reference points so the mutual information between them is high. This is not the case with the tracheal splitting, which had less distinct points so the mutual information is lower. The major error for the tracheal splitting lies in lung pairs 8, 9 and 10, which is mainly due to the large difference in the interslice distance between the fixed and test volumes.

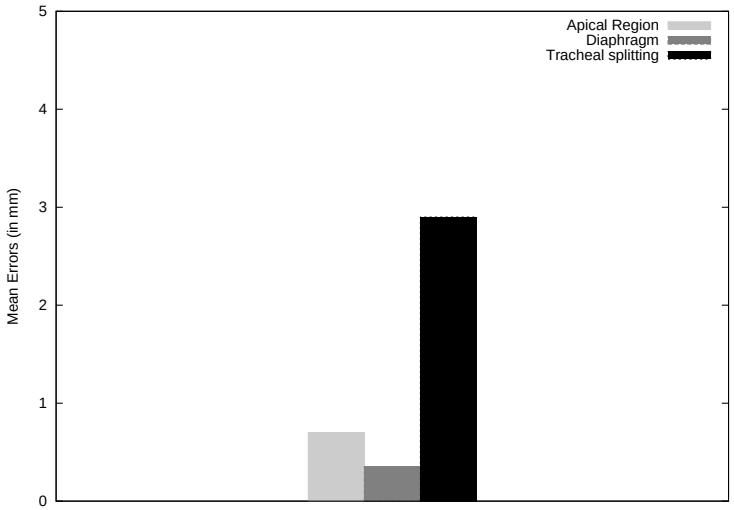

Figure 7: *Mean Error in lungs.*

5. PLUGIN IN FOR OSIRIX

An Osirix plugin was developed that can be seen in Figure 8. The user can easily tune the parameters such as grid size for deformable registration and the number of iterations required for both global and local registration algorithms. The number of iterations allows choosing a tradeoff between registration accuracy and computing time. The user can also choose to use only rigid registration, since we found that for most of brain images a simple rigid registration scheme allowed high registration accuracy. However, when local variations have to be captured, deformable registration schemes are suggested. The slice numbers are synchronized among all series.

6. CONCLUSIONS

The results in this paper show that fully automatic alignment of several volumes of images is possible with relatively high precision. Precision is lower in the case where compared volumes have large differences in inter slice distance and in slice thickness, which could be expected. Depending on the anatomic region and the partial overlap, the required registration algorithms can slightly vary. We compared the case of CT images of the lung and MRI brain images as examples. Computational complexity is another aspect to take into account and having several steps of registration starting from a lower resolution image can reduce this complexity. Brain images are relatively rigid and thus registration was easier than for the lungs where much soft tissue is involved and where anatomic differences between persons can be stronger. In the case where images of the same patient are compared this should not play a major role as anatomic variability is in this case low and even varying slice thicknesses or inter slice distances can be dealt with.

Our goal was to have a toolbox that can be adapted to various types of images and showing that these tools work for CT and MRI of two regions is only a first step. The mean error analyzed for the lungs was 3.95 mm and for the brain all slices could be perfectly registered albeit for only a small number of series.

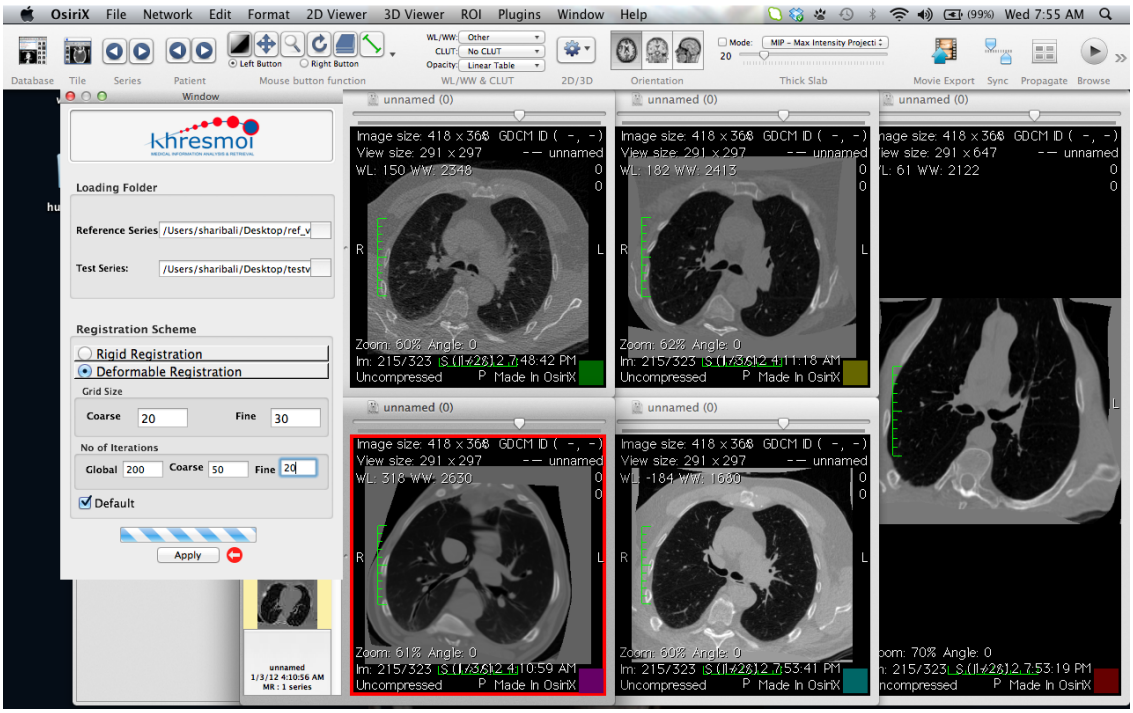

Figure 8: *A screenshot of the Osirix plugin. Registration results obtained using four test series (left) registered with a reference volume (right) with the parameters shown in the menus at the left.*

In the case of similar image series found with content–based visual retrieval, it seems important to include parameters that may reduce variability, such as adding the age and gender to the visual retrieval for similarity calculations and potentially also height and weight that might have a strong influence on the images. The current algorithm is only a starting point and evaluations on more anatomic regions seem necessary. A clinical evaluation is the final goal, also to show the advantages and inconveniences in using and automatic solution for alignment. For such an evaluation the Osirix plugin still needs to be improved. Plugins that require opening several image series are not easy to integrate into OsiriX. On the other hand such an integration is necessary to obtain any real impact of the final solution.

7. ACKNOWLEDGEMENTS

We would like to thank the EU for their funding in the context of the Khresmoi project (grant 257528) and the Swiss National Science foundation (grant 205321–130046).

REFERENCES

1. H. Müller, N. Michoux, D. Bandon, and A. Geissbuhler, "A review of content–based image retrieval systems in medicine–clinical benefits and future directions," *International Journal of Medical Informatics* **73**(1), pp. 1–23, 2004.
2. A. Rosset, L. Spadola, and O. Ratib, "OsiriX: An open–source software for navigating in multidimensional DICOM images," *Journal of Digital Imaging* **17**, pp. 205–216, September 2004.

3. G. Quellec, M. Lamard, G. Cazuguel, C. Roux, and B. Cochener, "Case retrieval in medical databases by fusing heterogeneous information," *IEEE Transactions on Medical Imaging* **30**, pp. 108–118, jan. 2011.
4. A. Depeursinge, A. Vargas, A. Platon, A. Geissbuhler, P.-A. Poletti, and H. Müller, "3D case–based retrieval for interstitial lung diseases," in *MCBR–CDS 2009: Medical Content–based Retrieval for Clinical Decision Support*, *Lecture Notes in Computer Science (LNCS)*, pp. 39–48, Springer, February 2010.
5. H. Müller, A. Rosset, A. Garcia, J.-P. Vallée, and A. Geissbuhler, "Benefits from content–based visual data access in radiology," *RadioGraphics* **25**, pp. 849–858, May 2005.
6. H. D. Tagare, C. Jaffe, and J. Duncan, "Medical image databases: A content–based retrieval approach," *Journal of the American Medical Informatics Association* **4**(3), pp. 184–198, 1997.
7. H. J. Lowe, I. Antipov, W. Hersh, and C. A. Smith, "Towards knowledge–based retrieval of medical images. The role of semantic indexing, image content representation and knowledge–based retrieval," in *Proceedings of the Annual Symposium of the American Society for Medical Informatics (AMIA)*, pp. 882–886, (Nashville, TN, USA), October 1998.
8. R. François, R. Fablet, and C. Barillot, "Robust statistical registration of 3D ultrasound images using texture information," in *Proceedings of the International Conference on Image Processing, 2003. ICIP 2003.*, **1**, pp. 581–584, September 2003.
9. D. Skerl, B. Likar, and F. Pernus, "A protocol for evaluation of similarity measures for rigid registration," *IEEE Transactions on Medical Imaging* **25**, pp. 779–791, June 2006.
10. J. N. Ulysses and A. Conci, "Measuring similarity in medical registration," in *17th International Conference on Systems, Signals and Image Processing*, *IWSSIP 2010*, June 2010.
11. W. M. Wells, P. Viola, H. Atsumi, S. Nakajima, and R. Kikinis, "Multi–modal volume registration by maximization of mutual information," *Medical Image Analysis* **1**(1), pp. 35–51, 1996.
12. P. Viola and W. M. Wells, "Alignment by maximization of mutual information," *International Journal of Computer Vision* **24**(2), pp. 137–154, 1997.
13. D. Rueckert, P. Aljabar, R. Heckemann, J. Hajnal, and A. Hammers, "Diffeomorphic registration using B–splines," in *Medical Image Computing and Computer-Assisted Intervention - MICCAI 2006*, R. Larsen, M. Nielsen, and J. Sporring, eds., *Lecture Notes in Computer Science* **4191**, pp. 702–709, Springer Berlin / Heidelberg, 2006.
14. D. Rueckert, L. I. Sonoda, C. Hayes, D. L. G. Hill, M. O. Leach, and D. J. Hawkes, "Non-rigid registration using free–form deformations: application to breast MR images," *IEEE Transactions on Medical Imaging* **18**, pp. 712–721, August 1999.
15. U. Bagci and L. Bai, "Multiresolution elastic medical image registration in standard intensity scale," in *Computer Graphics and Image Processing*, IEEE, ed., pp. 305–312, (Minas Gerais, Brazil), 2007.
16. K. Murphy, B. van Ginneken, J. M. Reinhardt, S. Kabus, D. K., X. Deng, and J. P. Pluim, "Evaluation of methods for pulmonary image registration: The EMPIRE10 study," in *MICCAI workshop on medical image analysis for the clinic*, pp. 11–22, (Beijing, China), 2010.